Minimizing emittance growth via low emittance transfer

Chuan Zhang*

GSI Helmholtz Centre for Heavy Ion Research, Planckstraße 1, D-64291 Darmstadt, Germany

(Received 13 June 2021; accepted 3 February 2022; published 9 March 2022)

The longitudinal-transverse coupling is an important source for space-charge-induced emittance growth in high intensity proton and ion linacs. Different from the equipartitioning method which tries to avoid the longitudinal-transverse coupling, a new design approach has been developed to minimize emittance growth via the low emittance transfer enabled by holding the ratio of longitudinal emittance to transverse emittance in the range of 0.9–1.4. Using a high intensity radio-frequency quadrupole accelerator as an example, a comparison between the new approach and the equipartitioning method has been made. Furthermore, input beams with non-nominal beam intensities and emittances have been applied to the designed accelerator. The simulation results show that the design obtained by following the new approach has a large tolerance for the off-design situations.

DOI: 10.1103/PhysRevAccelBeams.25.034201

I. INTRODUCTION

Space-charge-induced emittance growth is a big concern for designing high intensity proton and ion linacs, especially the radio-frequency quadrupole (RFQ) accelerators which are typically designed for the acceleration of low-velocity beams in the range of ∼0.01 to 0.06 (nowadays extended to 0.08) times the speed of light in vacuum c [1]. In this study, a new design approach to minimize emittance growth for high intensity RFQ accelerators is being introduced.

The RFQ accelerator is a kind of special accelerator that focuses, bunches and accelerates the beam only using the rf field. The essential parts of an RFQ accelerator are the four electrodes which are surrounding the beam axis and in alternating polarities. Figure 1 shows a cross-section view of a pair of adjacent RFQ electrodes and their surface electric-field components schematically, where a is the minimum electrode aperture of a unit cell (often abbreviated as "cell"), m is the electrode modulation, r_0 is the midcell electrode aperture, $L_c = \frac{\beta\lambda}{2}$ is the cell length, β is the synchronous-particle velocity relative to c, λ is the wave length, and U is the intervane voltage. In different positions of the RFQ, one can adjust a, m, U, and the synchronous phase φ_s to adapt the transverse and longitudinal electric-field components for meeting different demands on focusing, bunching, and acceleration, respectively. These are the main parameters to design an RFQ structure.

*c.zhang@gsi.de

As RFQs typically work for very low-velocity (Lorentz factor $\gamma \approx 1$) beams, it allows describing the motion of a particle with charge q and mass m_0 in all three planes with the following equation:

$$m_0\ddot{u} = F_{\mathrm{rf,u}} + F_{\mathrm{sc,u}}, \tag{1}$$

where $\ddot{u} = \frac{d^2u}{dt^2}$, $F_{\mathrm{rf,u}} = qE_{\mathrm{rf,u}}$ is the external electric-field force, and $F_{\mathrm{sc,u}} = qE_{\mathrm{sc,u}}$ is the space-charge force from the self-field of particles (the contribution from the self-magnetic field can be ignored at $\gamma \approx 1$ [2]). In Eq. (1), u represents x, y or z (as a subscript, it represents the direction; otherwise, it represents the displacement in that direction). Analytically, the external electric-field components can be obtained from the well-known two-term potential function [3,4] proposed by the RFQ inventors, Kapchinskii and Teplyakov, while the space-charge electric-field components in a beam bunch can be obtained using a 3D uniform ellipsoid model (with linear space-charge-force components) proposed by Lapostolle [1,5].

Using the longitudinal position on the beam axis s instead of t as the independent variable, we may rewrite Eq. (1) as

$$u'' + K_{\mathrm{u}}(s)u = 0, \tag{2}$$

where $u'' = \frac{d^2u}{ds^2}$ and $K_{\mathrm{u}}(s)$ denotes the focusing strength provided by all (external and self-field) applied forces.

Based on the smooth approximation [1], the phase advance per unit length k_{u} is related to $K_{\mathrm{u}}(s)$ by $k_{\mathrm{u}} = \sqrt{|K_{\mathrm{u}}(s)|}$ and the phase advance per focusing period L_{p} (for RFQs: $L_{\mathrm{p}} = \beta\lambda$) is $\sigma_{\mathrm{u}} = k_{\mathrm{u}}L_{\mathrm{p}}$. Only considering the external forces, one can get the phase advance per focusing period without space charge from the external electric-field components as

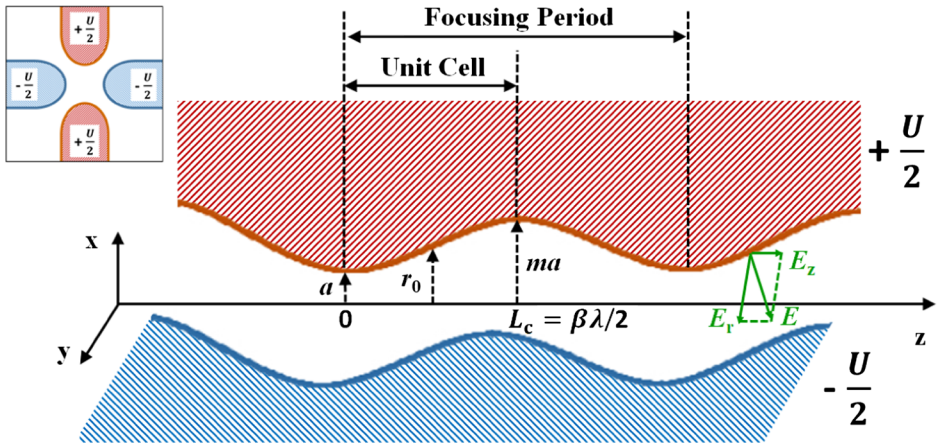

FIG. 1. Schematic cross-section view of a pair of adjacent RFQ electrodes and their surface electric-field components.

$$\sigma_{0t} = \sqrt{\frac{B^2}{8\pi^2} + \Delta_{rf}} \tag{3}$$

$$\sigma_{0l} = \sqrt{-2\Delta_{rf}} \tag{4}$$

with $B \equiv \frac{qXU\lambda^2}{m_0c^2a^2}$, $\Delta_{rf} \equiv \frac{\pi^2 qAU \sin\varphi_s}{2m_0c^2\beta^2}$, $X \equiv \frac{I_0(ka)+I_0(kma)}{m^2I_0(ka)+I_0(kma)}$, $A \equiv \frac{m^2-1}{m^2I_0(ka)+I_0(kma)}$, and $k = \frac{\pi}{L_c} = \frac{2\pi}{\beta\lambda}$. For Eqs. (3) and (4), the subscripts "0," "t," and "l" refer to zero current, the transverse planes (x and y), and the longitudinal plane (z), respectively.

Equation (2) shows that the particle displacement satisfies the equation of a simple harmonic oscillator in both transverse and longitudinal planes. The relationship between the angular oscillation frequency $\omega_{o,u}$ and σ_u is $\omega_{o,u} = \frac{\sigma_u c}{\lambda}$.

To calculate the phase advance with space charge analytically, one can follow Sacherer's procedure [6] to convert the single-particle equation, Eq. (2), to the following root mean square (rms) envelope equation:

$$R_u'' + K_u(s)R_u - \frac{\varepsilon_u^2}{R_u^3} = 0, \tag{5}$$

where $R_u = \sqrt{\overline{u^2}}$ is the rms beam size, $K_u(s)$ is the focusing strength for the beam (in the above equation, the external-focusing term and the space-charge term are combined into one for simplifying the analysis), and ε_u is the unnormalized rms emittance defined by $\varepsilon_u \equiv \sqrt{\overline{u^2}\,\overline{u'^2} - \overline{uu'}^2}$. This rms envelope equation is widely applicable for all particle distributions [6]. For matched beams ($R_u'' = 0$) [7], one obtains k_u and σ_u as

$$k_u = \frac{\varepsilon_u}{R_u^2} \tag{6}$$

$$\sigma_u = \frac{\varepsilon_u\beta\lambda}{R_u^2}. \tag{7}$$

More generally, the phase advance with space charge can be obtained from the beam dynamics simulation with the following definition [1]:

$$\sigma_u \equiv \int_0^{L_p} \frac{ds}{\tilde{\beta}_u(s)} = \int_0^{L_p} \frac{\varepsilon_u}{R_u^2} ds, \tag{8}$$

where $\tilde{\beta}_u$ is one of the Twiss parameters and satisfies $R_u = \sqrt{\tilde{\beta}_u\varepsilon_u}$.

The longitudinal and transverse oscillations of the beam are not independent of each other. When certain conditions are met, the longitudinal and transverse coupling can occur. In 1968, the longitudinal-transverse coupling was identified by Chasman as an important mechanism for space-charge-induced emittance growth in high intensity proton linacs [8] and Lapostolle proposed that this kind of emittance growth could be minimized by equipartitioning [9]. In 1981, Jameson published the equipartitioning principle (EP) and suggested minimizing space-charge-induced emittance growth by removing free oscillation energy (often abbreviated as "free energy") between the transverse and longitudinal degrees of freedom [10]. As mentioned above, the motion of the beam particle in the RFQ satisfies the equation of a simple harmonic oscillator in both transverse and longitudinal planes. The total oscillation energy of a simple harmonic oscillator is

$$E_{total} = \frac{1}{2}m_0\omega_o^2R^2 \tag{9}$$

with ω_o being the angular oscillation frequency and R being the oscillation amplitude which is the rms beam size for a beam. No free oscillation energy implies a balance of the longitudinal and transverse oscillation energies i.e.,

$$\frac{E_{\mathrm{total,l}}}{E_{\mathrm{total,t}}} = \frac{\omega_{\mathrm{o,l}}^2 R_{\mathrm{l}}^2}{\omega_{\mathrm{o,t}}^2 R_{\mathrm{t}}^2} = 1. \tag{10}$$

Substituting $\omega_{\mathrm{o,u}} = \frac{\sigma_{\mathrm{u}} c}{\lambda}$ and Eq. (7) into Eq. (10), we get the following EP equation:

$$\frac{\varepsilon_{\mathrm{l}}\sigma_{\mathrm{l}}}{\varepsilon_{\mathrm{t}}\sigma_{\mathrm{t}}} = 1. \tag{11}$$

Also in 1981, Hofmann reported the stability thresholds for different coupling modes in linear devices [11]. The calculation was performed using the Vlasov equation for an initial Kapchinskii-Vladimirskii distribution with arbitrary emittance ratios, tune ratios, and intensity [11]. These thresholds had been originally obtained for continuous beams in the two transverse directions, but it was found that they could be also applied to investigate the longitudinal-transverse emittance transfer in bunched beams [12]. Hofmann visualized the thresholds including the growth rate of coupling resonance in the form of charts and suggested that these stability charts could give a useful orientation for controlling the longitudinal-transverse coupling in linacs [13].

Equation (11) implies $\frac{\sigma_{\mathrm{l}}}{\sigma_{\mathrm{t}}} = \frac{\varepsilon_{\mathrm{t}}}{\varepsilon_{\mathrm{l}}}$, where $\frac{\sigma_{\mathrm{l}}}{\sigma_{\mathrm{t}}}$ is the tune ratio (i.e., the ratio of longitudinal phase advance σ_{l} to transverse phase advance σ_{t}) and $\frac{\varepsilon_{\mathrm{t}}}{\varepsilon_{\mathrm{l}}}$ is the ratio of transverse emittance ε_{t} to longitudinal emittance ε_{l}. Figure 2 shows several Hofmann charts for different emittance ratios in the range of $\frac{\varepsilon_{\mathrm{l}}}{\varepsilon_{\mathrm{t}}} = 0.9$–$1.4$, where the abscissa is the tune ratio $\frac{\sigma_{\mathrm{l}}}{\sigma_{\mathrm{t}}}$ and the ordinate is the tune depression ratio $\frac{\sigma_{\mathrm{t}}}{\sigma_{0\mathrm{t}}}$ or $\frac{\sigma_{\mathrm{l}}}{\sigma_{0\mathrm{l}}}$. They are the same as $\frac{k_{\mathrm{l}}}{k_{\mathrm{t}}}$ and $\frac{k_{\mathrm{t}}}{k_{0\mathrm{t}}}$ ($\frac{k_{\mathrm{l}}}{k_{0\mathrm{l}}}$) used by Hofmann originally, because $\frac{\sigma_{\mathrm{l}}}{\sigma_{\mathrm{t}}} = \frac{k_{\mathrm{l}}}{k_{\mathrm{t}}}$ and $\frac{\sigma_{\mathrm{t}}}{\sigma_{0\mathrm{t}}} = \frac{k_{\mathrm{t}}}{k_{0\mathrm{t}}}$ ($\frac{\sigma_{\mathrm{l}}}{\sigma_{0\mathrm{l}}} = \frac{k_{\mathrm{l}}}{k_{0\mathrm{l}}}$). A smaller tune depression ratio means stronger space charge effects and vice versa.

On a Hofmann chart, the darker the color is, the higher the growth rate of coupling resonance is. The major resonance peaks usually appear at the positions where $\frac{\sigma_{\mathrm{l}}}{\sigma_{\mathrm{t}}} = \frac{i}{j}$ (i and j are

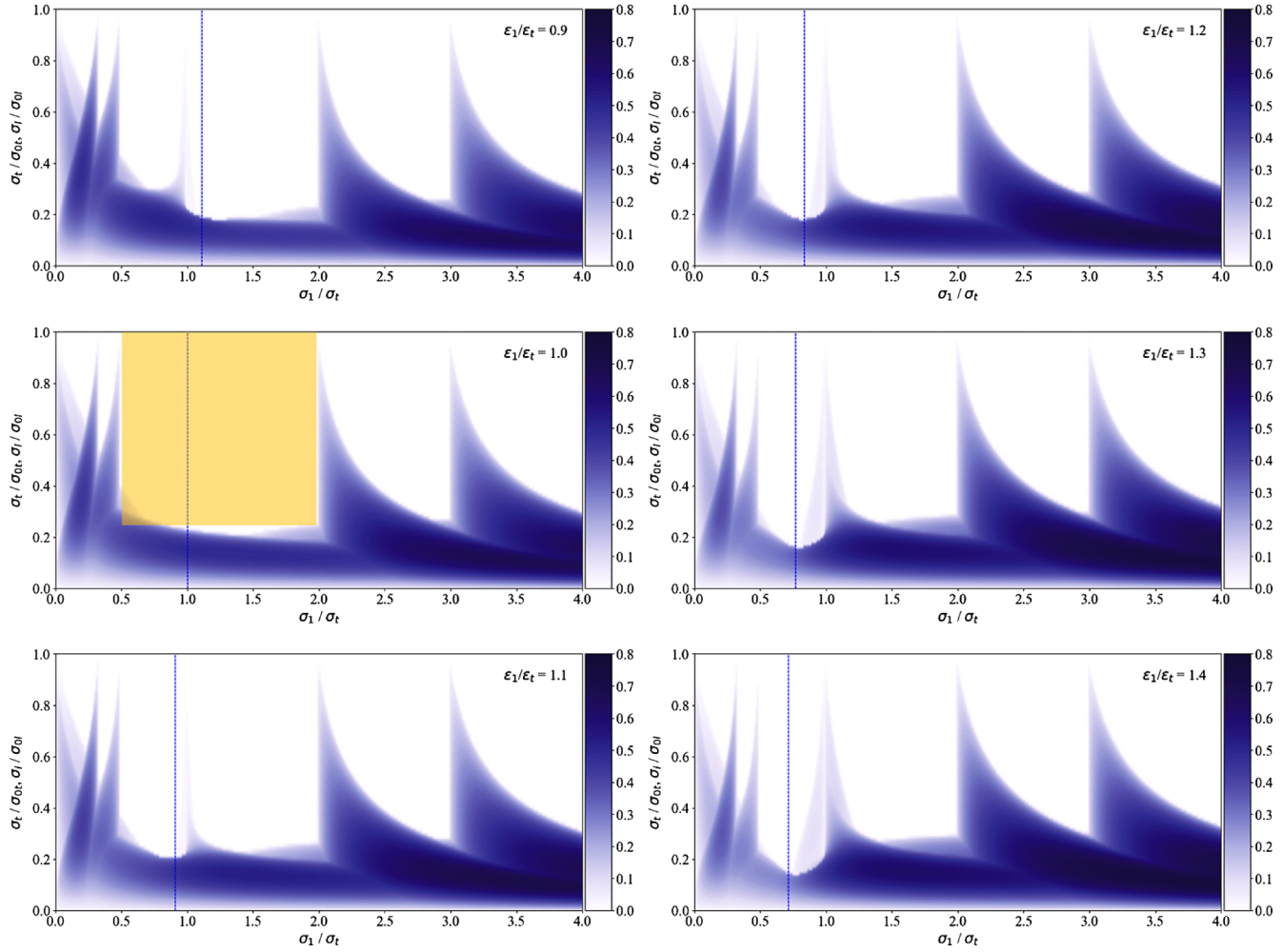

FIG. 2. Hofmann charts for the emittance ratios $\frac{\varepsilon_{\mathrm{l}}}{\varepsilon_{\mathrm{t}}}$ in the range of 0.9–1.4. The blue dashed lines mark the locations where the EP equation is satisfied. The charts were generated using the TraceWin code [14] with the colorbar showing the growth rate of coupling resonance.

integers), e.g., $\frac{\sigma_l}{\sigma_t} = \frac{1}{2}$, $\frac{1}{1}$, and $\frac{2}{1}$, while the maximum spread of the safe tune depression is always available at a location where the EP equation is satisfied (see the blue dashed lines in Fig. 2). On a Hofmann chart for a certain emittance ratio $\frac{\varepsilon_l}{\varepsilon_t}$, if originally there is a resonance peak located at $\frac{\sigma_l}{\sigma_t} = \frac{\varepsilon_l}{\varepsilon_t}$, this peak will vanish due to the lack of the free energy to drive resonances. However, this peak disappears only in the case where the EP condition is exactly met. Any deviation will result in the return of the vanished peak. The larger the deviation is, the more the peak regrows. For example, the $\frac{\sigma_l}{\sigma_t} = 1.0$ resonance peak disappears on the $\frac{\varepsilon_l}{\varepsilon_t} = 1.0$ Hofmann chart, but it grows again on the neighboring charts gradually (see Fig. 2).

II. NEW DESIGN APPROACH: MINIMIZING EMITTANCE GROWTH VIA LOW EMITTANCE TRANSFER

It is true that if the EP condition is satisfied, the coupling resonance can be maximally avoided. However, free energy does not necessarily cause resonances. It can be seen in Fig. 2 that there is a sufficient clean (resonance-free) area on a Hofmann chart besides the EP line. In addition, usually emittance transfer cannot be avoided completely in reality, and a changed emittance ratio will move the EP line in the tune space. Therefore, it makes more sense to choose the clean area on the Hofmann charts instead of sticking on the EP line for the beam motion.

A previous study [15] showed that the Hofmann chart which met the condition given in Eq. (12) could provide a quasirectangular clean area with wide ranges of tune ratio ($\frac{\sigma_l}{\sigma_t} = 0.5$–$2.0$) and tune depression ratio ($\frac{\sigma}{\sigma_0} = \sim 0.25$–$1.0$), respectively. To minimize the emittance transfer, it was recommended using this "safe rectangle" (see the area marked in orange in Fig. 2) to the greatest extent for the beam motion [15]:

$$\frac{\varepsilon_l}{\varepsilon_t} = 1.0. \tag{12}$$

However, it will be very demanding to hold the emittance ratio $\frac{\varepsilon_l}{\varepsilon_t}$ at one in the real machines. A more practical design guideline is to hold $\frac{\varepsilon_l}{\varepsilon_t}$ close to one. Although the $\frac{\sigma_l}{\sigma_t} = 1.0$ resonance peak will regrow when a deviation from $\frac{\varepsilon_l}{\varepsilon_t} = 1.0$ starts, fortunately the $\frac{\sigma_l}{\sigma_t} = 1.0$ resonance peak would not be significant and its resonance growth rates would be low, if $\frac{\varepsilon_l}{\varepsilon_t}$ can be held in the range of $0.9 \leq \frac{\varepsilon_l}{\varepsilon_t} \leq 1.4$ (see Fig. 2).

An emittance ratio range leading to low emittance transfer has been determined. The next steps will be how to put and maintain the tune trajectories of the beam inside this $\frac{\varepsilon_l}{\varepsilon_t}$ range and how to take advantage of the low emittance transfer for minimizing emittance growth.

Typically, an RFQ accelerator receives a continuous beam from an ion source or a low energy beam transport section with very small energy spread ΔW_{in} but very large phase spread $\Delta\varphi_{\mathrm{in}}$. For RFQ beam dynamics design studies, therefore, it is usually assumed that $\Delta W_{\mathrm{in}} = 0$ and $\Delta\varphi_{\mathrm{in}} = \pm 180°$, respectively, which leads to $\varepsilon_{\mathrm{l,in}} = 0$. From the longitudinal beam dynamics point of view, the input beam will go through three sequential stages in an RFQ designed using the new four section procedure (NFSP) [16]: (i) The first stage of bunching (initial bunching) with maximum separatrix starts from a continuous beam to form an initial bunch with a full 360° phase acceptance ($\varphi_s = -90°$). During this period, ε_l is being increased from 0 to a certain value which can be regarded as the "actual" $\varepsilon_{\mathrm{l,in}}$. Meanwhile, $\frac{\sigma_l}{\sigma_t}$ also starts to increase from 0. Before the beam bunch is initially formed, no significant emittance transfer between the longitudinal and transverse planes will occur. (ii) The second stage of bunching with small acceleration continues decreasing the phase spread of the initial bunch to be close to the target value. As the longitudinal electric field is still mainly used for bunching in this stage, the acceleration is small. Therefore, this part is most critical for space charge, especially at its end. During the longitudinal beam compression, $\frac{\sigma_l}{\sigma_t}$ is increasing and emittance transfer can occur from the longitudinal plane to the transverse ones. (iii) The main acceleration stage with a final bunching starts the real acceleration for the bunched beam and makes a final bunching to tune the output beam parameters as desired. Consequently, the longitudinal focusing force as well as the transverse defocusing effect will be weakened naturally. In this stage, $\frac{\sigma_l}{\sigma_t}$ will start decreasing again and the emittance transfer will also reverse the direction (i.e., the emittance transfer will occur from the transverse planes to the longitudinal one).

The typical evolution of the main RFQ design parameters for these three stages is schematically shown in Fig. 3.

Dividing an RFQ also into three stages, a new approach so-called minimizing emittance growth via low emittance transfer (MEGLET) is being proposed as a further development of the NFSP method. According to the evolution of the tune trajectories on the Hofmann chart, the new three stages are divided as follows: (i) Before entering the "safe rectangle." It includes the initial bunching and the starting part of the second stage of bunching with $\frac{\sigma_l}{\sigma_t} < 0.5$. One can choose a relatively large $\frac{\varepsilon_l}{\varepsilon_t}$ in the range of 0.9–1.4, e.g., 1.3, for the end of the initial bunching, because the subsequent emittance transfer can lower $\frac{\varepsilon_l}{\varepsilon_t}$ down to ~1.0 when the tune trajectories are approaching the "safe rectangle". (ii) "Traveling" inside the "safe rectangle." It covers the part around the end of the second stage of bunching with $0.5 \leq \frac{\sigma_l}{\sigma_t} \leq 2.0$. This stage is most critical for space charge, especially at high intensities, so this part of the tune trajectories should be well kept inside the "safe rectangle". It is also important to keep the oscillation of the tune trajectories at the turning point (where the tune trajectories are turning around) away from the position $\frac{\sigma_l}{\sigma_t} = 1$ where the

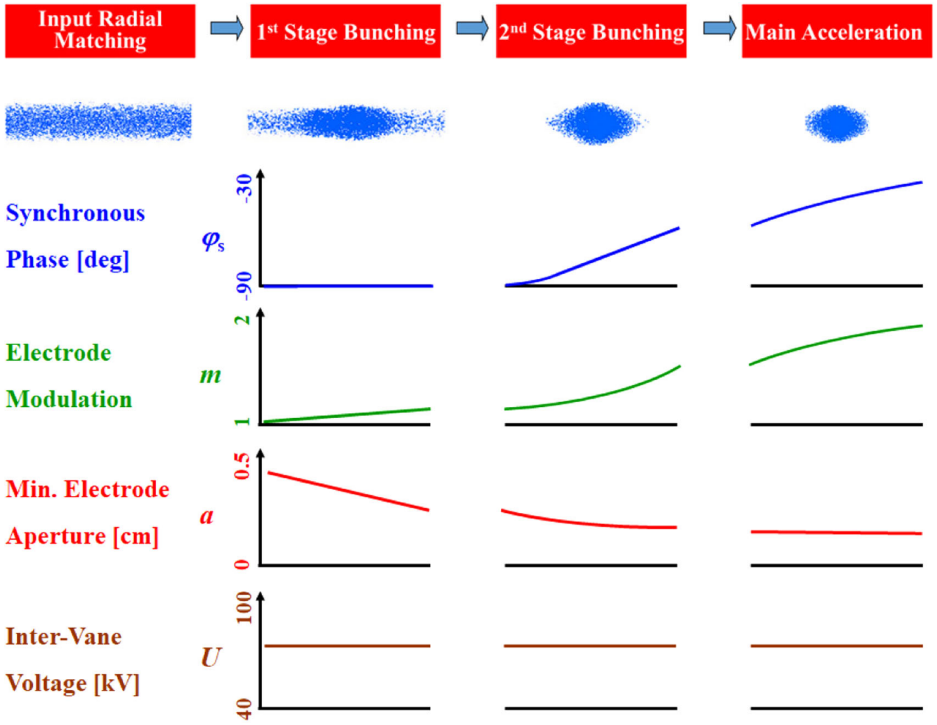

FIG. 3. Schematic plot for the variation of the main parameters along an NFSP-style RFQ (marked with some typical values).

resonance peak can regrow. A proper position for having the oscillation could be at $\frac{\sigma_l}{\sigma_t} = 1.2$. (iii) After leaving the "safe rectangle." In this stage, the tune trajectories will go back to the $\frac{\sigma_l}{\sigma_t} < 0.5$ region and move further towards $\frac{\sigma_l}{\sigma_t} = 0$, and at the same time the emittance transfer will reverse the direction and increase $\frac{\varepsilon_l}{\varepsilon_t}$. It can be seen in Fig. 2 that the growth rates of the $\frac{\sigma_l}{\sigma_t} \leq 0.5$ resonance peaks are low and they are decreasing with an increasing $\frac{\varepsilon_l}{\varepsilon_t}$. Therefore, the emittance transfer will be not very significant here. The low emittance transfer will be favorable to help bringing the ε_l, ε_t, and $\frac{\varepsilon_l}{\varepsilon_t}$ values back to the levels before the emittance transfer starts.

In this way, the originally harmful emittance transfer can be used as a beneficial tool for minimizing the emittance growth in both transverse and longitudinal planes.

In Fig. 4, the NFSP stages and the MEGLET stages (except the input radial matching stage which is typically only several cells long) are shown together schematically. In total, there are six key points for dividing all these stages and for designing a MEGLET-style RFQ accelerator section by section. The target values $\frac{\sigma_l}{\sigma_t}$ and $\frac{\varepsilon_l}{\varepsilon_t}$ will be

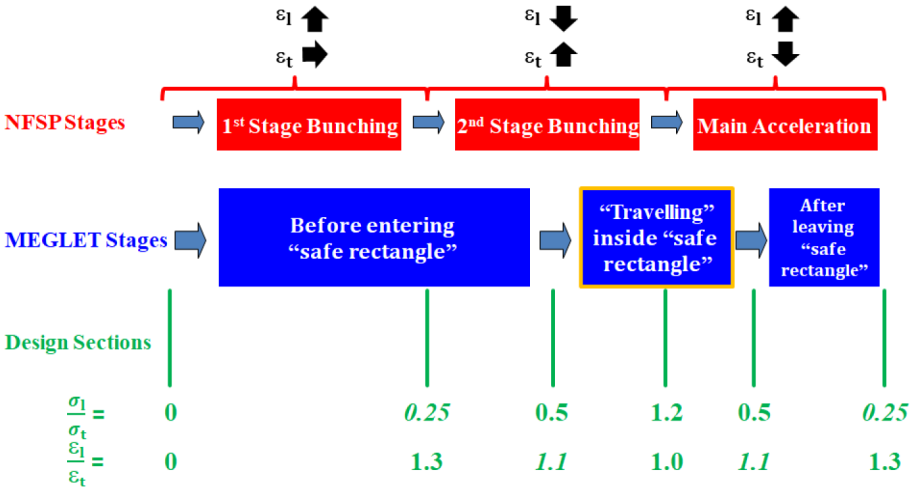

FIG. 4. Design sections for an MEGLET-style RFQ (marked with some typical target values for the tune ratio and the emittance ratio; for the numbers in italics, relatively larger deviations can be acceptable).

obtained from the simulation. The tune ratio at zero current $\frac{\sigma_{0l}}{\sigma_{0t}}$ is determined by the structure-related parameters (e.g., a, m, U, and φ_s) and can be calculated by using Eqs. (3) and (4). Therefore, it is convenient to take $\frac{\sigma_{0l}}{\sigma_{0t}}$ as a good estimation of $\frac{\sigma_l}{\sigma_t}$ for the design. The typical evolution of the structure-related parameters along the RFQ can be found in Fig. 3. To avoid abrupt changes of the parameters, the transitions between the sections can be properly smoothed.

III. MEGLET RFQ DESIGN AND COMPARISON WITH THE EP METHOD

To apply the new design approach, a 324 MHz, 3 MeV proton RFQ has been taken as an example. For the convenience of description, this proton RFQ is hereafter also referred to as the MEGLET RFQ. Table I lists its basic parameters. The design goal for the MEGLET RFQ is to achieve high beam transmission efficiency T using a short structure length L with the focus especially on minimizing emittance growth.

Table II lists the 3 MeV H^+ or H^- RFQ accelerators constructed or being constructed worldwide in the 21st century. From the beam dynamics point of view, the difference between H^+ and H^- ions is ignorable. It can be seen that the chosen basic parameters of the MEGLET RFQ are representative. Except the intervane voltage, they are identical to those of the J-PARC epRFQ [17] which was designed as a "fully equipartitioned" machine. This will allow a comparison between the MEGLET approach and the EP method.

TABLE I. Basic design parameters of the MEGLET RFQ.

Parameter	Value
Ion species	H^+
Frequency f [MHz]	324
Input energy W_{in} [keV]	50
Output energy W_{out} [MeV]	3.0
Input beam intensity I_{in} [mA]	60
Input emittance $\varepsilon_{t,in,n,rms}$ [π mm mrad]	0.20
Intervane voltage U [kV]	75

Following the new approach, the beam dynamics design of the MEGLET RFQ has been made. Figure 5 shows the evolution of the main design parameters along the MEGLET RFQ.

The beam dynamics simulation of the MEGLET RFQ has been performed using the PARMTEQM code [24] with 10^5 input macroparticles. The same as for the J-PARC epRFQ, a waterbag-type input distribution has been adopted for the MEGLET RFQ.

It can be seen in Fig. 6 that no matter with or without space charge, the phase advance values along the MEGLET RFQ are all smaller than 45°. They are well below the stopbands of both the second to fourth order parametric resonances and the fourth and sixth order single-particle resonances [25], so for the MEGLET RFQ, only the longitudinal-transverse coupling resonance is important.

Figure 7 shows the beam trajectories of the MEGLET RFQ in the tune space, where the red and green curves are corresponding to the transverse and longitudinal tune depression ratios, $\frac{\sigma_t}{\sigma_{0t}}$ and $\frac{\sigma_l}{\sigma_{0l}}$, as functions of tune ratio $\frac{\sigma_l}{\sigma_t}$, respectively. The arrows indicate the moving directions of the tune trajectories. Each arrow represents one step. For small steps, the size of the arrows has been reduced to avoid crowding the figure. As the tune trajectories enter and leave the "safe rectangle" at cell 95 and cell 163, respectively, the MEGLET RFQ can be divided into the following three stages: (i) stage 1: from the RFQ entrance up to cell 95; (ii) stage 2: between cell 95 and cell 163; (iii) stage 3: the remaining part after cell 163.

In Fig. 8, the longitudinal and transverse emittances are plotted as functions of cell number (the cell number is the serial number of a unit cell), where the emittance curves for 99% of the particles are used to show the performance of the main beam by excluding 1% of the outermost particles.

TABLE II. Modern 3 MeV H^+ or H^- RFQ accelerators in the world (sorted by the input beam intensity used for the beam dynamics simulation).

Parameter	KOMAC (PEFP) [18]	CSNS [19]	J-PARC RFQ-III [20]	J-PARC epRFQ [17]	CPHS [21]	CERN Linac4 [22]	FAIR p-Linac [23]
Ion species	H^+	H^-	H^-	H^-	H^+	H^-	H^+
f [MHz]	350	324	324	324	325	352.2	325.224
W_{in} [keV]	50	50	50	50	50	45	95
W_{out} [MeV]	3.0	3.0	3.0	3.0	3.0	3.0	3.0
I_{in} [mA]	22	40	60	60	60	70	100
$\varepsilon_{t,in,n,rms}$ [π mm mrad]	0.20	0.20	0.20	0.20	0.20	0.25	0.30
U [kV]	85	80	81	61.3–143	60–135	78	88.43
$\varepsilon_{t,out,n,rms}$ [π mm mrad]	0.22	0.20	0.21	0.24	0.25	0.25	0.33
$\varepsilon_{l,out,n,rms}$ [π MeV deg]	0.112	0.1143	0.11	0.11	0.14	0.13	0.20
L [m]	3.21	3.603	3.623	3.073	2.969	3.06	3.3
T [%]	98.3	97.1	98.5	99.1	97.2	95.0	88.5

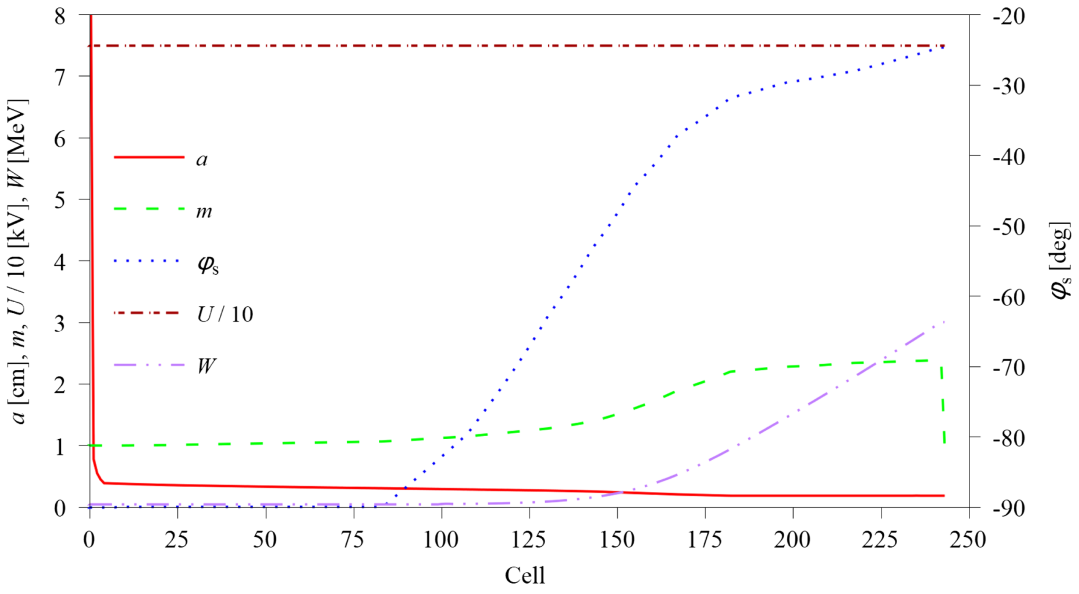

FIG. 5. Main design parameters of the MEGLET RFQ, where a is the minimum electrode aperture, m is the electrode modulation, φ_s is the synchronous phase, U is the intervane voltage, and W is the beam energy.

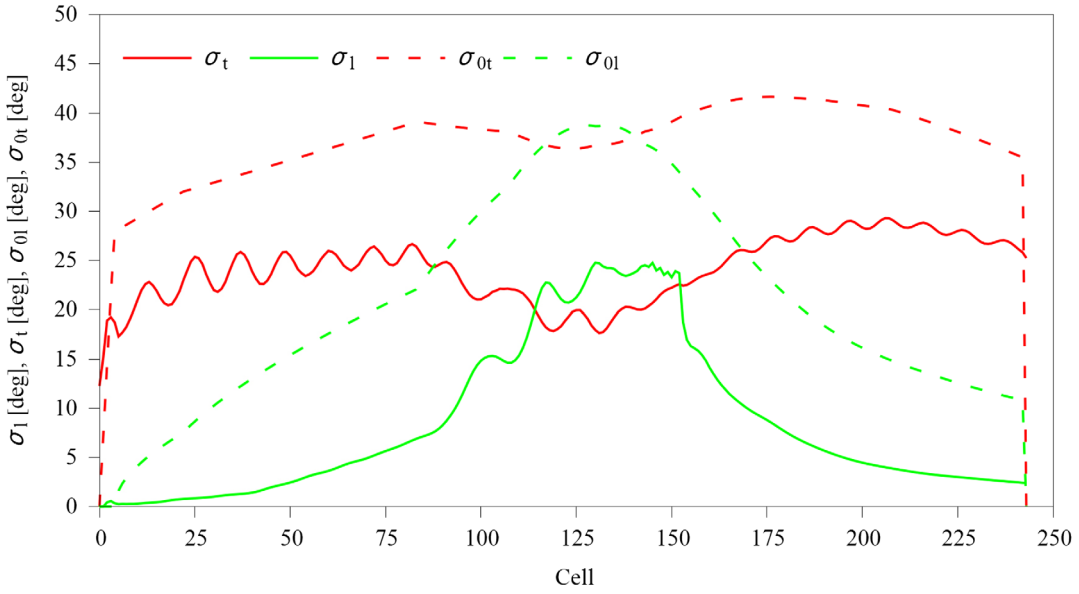

FIG. 6. Phase advance values with and without space charge along the MEGLET RFQ.

In the figure, all emittances are normalized with the unit of π mm mrad (after the normalization, the emittance ratio is kept unchanged, i.e., $\frac{\varepsilon_{l,n}}{\varepsilon_{t,n}} = \frac{\varepsilon_l}{\varepsilon_t}$). An often adopted unit of the longitudinal emittance is π MeV deg for linacs. The conversion formula for the longitudinal emittance unit from π MeV deg to π mm mrad is

$$\varepsilon_{l,n}[\pi\,\text{mm mrad}] = \frac{10^6}{360}\frac{\lambda[\text{m}]}{E_0[\text{MeV}]}\varepsilon_{l,n}[\pi\,\text{MeV deg}], \quad (13)$$

where E_0 is the rest energy of the beam particle in MeV.

Figure 8 shows that the formation of the initial beam bunch is done around cell 75 where the synchronous phase starts leaving −90° (see Fig. 5). The emittance ratio $\frac{\varepsilon_l}{\varepsilon_t}$ (in this study, it always refers to $\frac{\varepsilon_{l,100\%}}{\varepsilon_{t,100\%}}$ or $\frac{\varepsilon_{l,n,100\%}}{\varepsilon_{t,n,100\%}}$) at this position has been chosen as ∼1.3. Afterwards, the emittance transfer occurs from the longitudinal plane to the transverse ones, so the emittance ratio is being decreased and reaches ∼1.1 at the end of stage 1. In stage 2, the $\varepsilon_{l,n,100\%}$ curve starts to have a "jump" around cell 135 (see Fig. 8) where the real acceleration starts (see Fig. 5). This "jump" is caused by less than 1% of the particles which are outside of the separatrix and

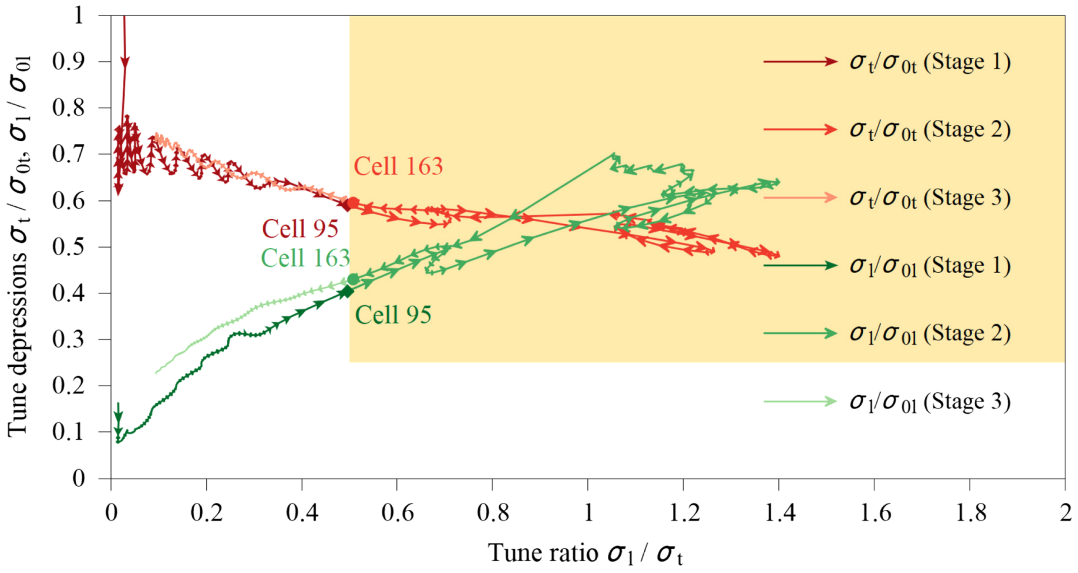

FIG. 7. Evolution of tune depression ratios along the MEGLET RFQ. The tune trajectories of the three stages are shown in red (transverse) and green (longitudinal) colors from dark to light. The "safe rectangle" marked in orange covers stage 2 where the space charge effects are most critical.

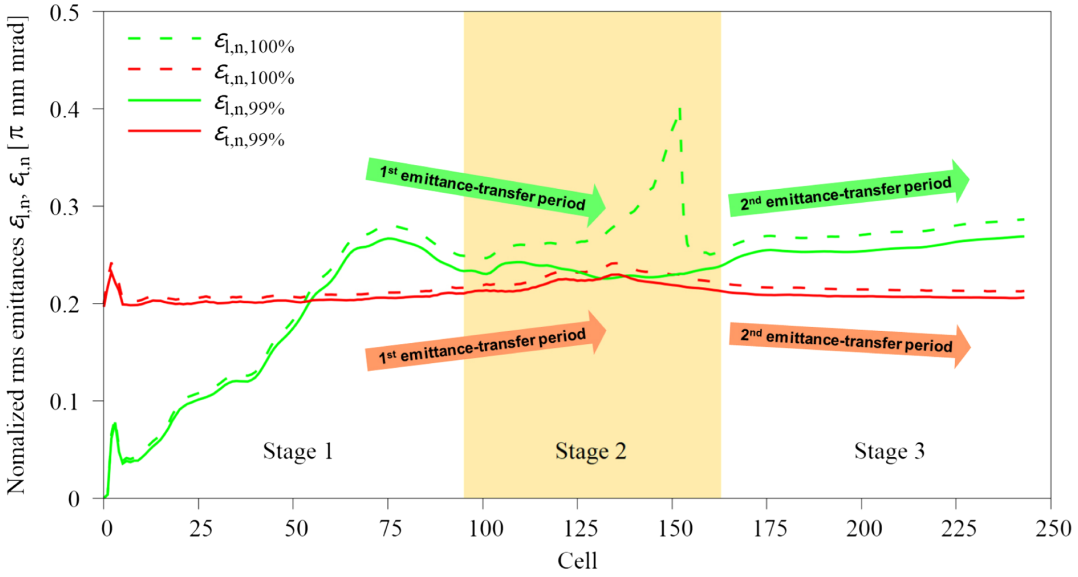

FIG. 8. Evolution of longitudinal and transverse emittances for 100% and 99% of particles along the MEGLET RFQ.

cannot catch the right acceleration. After they are lost, the $\varepsilon_{l,n,100\%}$ curve comes back to normal again. The real acceleration also reverses the direction of the emittance transfer so that the transverse and longitudinal emittances will be decreased and increased, respectively. "Protected" by the "safe rectangle," the emittance transfer in the whole stage 2 is relatively low and the emittance ratio at the end of this stage can be still held at ~1.1. Entering into the third stage, the beam will see the $\frac{\sigma_l}{\sigma_t} \leq 0.5$ resonance peaks again, so the emittance transfer will become stronger. However, Fig. 2 shows that the growth rates of the $\frac{\sigma_l}{\sigma_t} \leq 0.5$ resonance peaks on the Hofmann charts for $\frac{\varepsilon_l}{\varepsilon_t} = 1.1$–$1.4$ are relatively low and they are decreasing with an increasing $\frac{\varepsilon_l}{\varepsilon_t}$. Therefore, the emittance transfer in this stage will be slow. Figure 8 shows that at the exit of the MEGLET RFQ, both transverse and longitudinal emittances values are very close to those at cell 75 (before the emittance transfer starts), which means there is almost no emittance growth at the end. Shown in Fig. 9, the emittance ratio $\frac{\varepsilon_l}{\varepsilon_t}$ is well inside the range from 0.9 to 1.4 for most positions along the MEGLET RFQ.

The main simulation results of the MEGLET RFQ are summarized in Table III. The RFQ length L is about 3 m

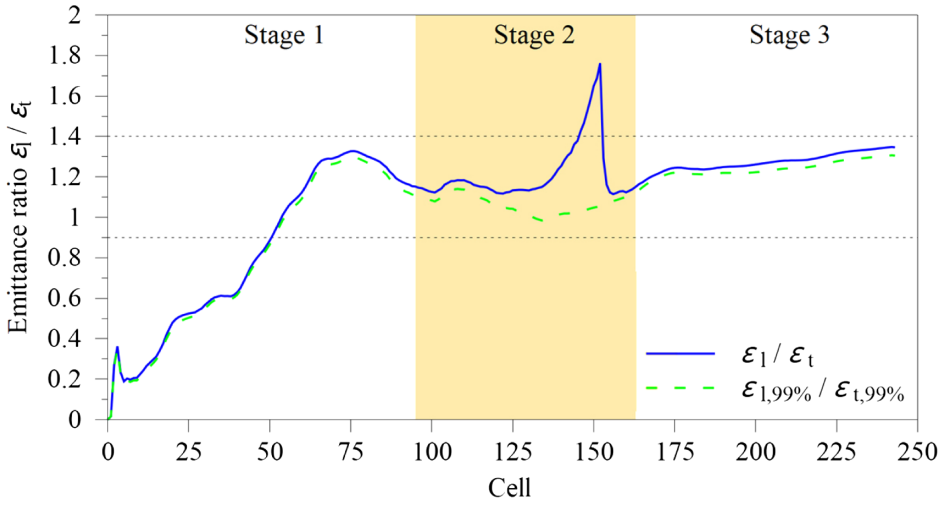

FIG. 9. Emittance ratio $\frac{\varepsilon_l}{\varepsilon_t}$ as a function of cell number.

and the beam transmission efficiency is 99.1%. Both are very comparable to those of the J-PARC epRFQ.

As the J-PARC epRFQ uses a nonconstant intervane voltage U, one needs to find an equivalent value for the comparison. The specific shunt impedance of an RFQ, R_p, is defined as

$$R_p = \frac{U^2 L}{P_c}, \tag{14}$$

where P_c is the rf power consumption. For the J-PARC epRFQ, the nominal P_c is 380 kW [26]. Because the J-PARC epRFQ and its predecessor, the J-PARC RFQ III [20], have the same frequency and similar design specifications, it is appropriate to assume that the two RFQs have the same R_p value. For the J-PARC RFQ III, $P_c = 400$ kW, $U = 81$ kV, and $L = 3.623$ m [20,27]. Based on all these data, the calculated equivalent intervane voltage for the J-PARC epRFQ is 85.7 kV which is ~14% higher than that adopted for the MEGLET RFQ.

For the J-PARC epRFQ, most of the tune trajectories have been indeed successfully concentrated with the EP line as the focus (see the fifth figure in [17]). However, the tune trajectories intensively oscillate around $\frac{\sigma_l}{\sigma_t} = 0.77$, the EP line for $\frac{\varepsilon_l}{\varepsilon_t} = 1.3$, and touch the main resonance peak at $\frac{\sigma_l}{\sigma_t} = 1.0$ many times (especially the transverse tune trajectory) so that the resonance can be accumulated. It can be seen in the second figure in [17] that the transverse emittance is gradually increasing along the J-PARC epRFQ and $\frac{\varepsilon_l}{\varepsilon_t}$ is not constant after the shaper but varies within the range of 1.2–1.5. In the MEGLET case, the tune trajectories have much less oscillations with much smaller amplitudes (see Fig. 7). Its main oscillation has been well confined around $\frac{\sigma_l}{\sigma_t} = 1.2$ in order to avoid touching the $\frac{\sigma_l}{\sigma_t} = 1.0$ major resonance peak repeatedly. More importantly, the MEGLET approach can use two emittance-transfer periods to bring both longitudinal and transverse output emittance values back to the levels before the emittance-transfer periods (see Fig. 8).

In this way, the MEGLET RFQ reaches smaller output emittance values in both transverse and longitudinal planes (see Table III).

TABLE III. Main design results of the MEGLET RFQ.

Parameter	MEGLET RFQ	J-PARC epRFQ [17]
Ion species	H^+	H^-
f [MHz]	324	324
W_{in} [keV]	50	50
W_{out} [MeV]	3.0	3.0
U [kV]	75	61.3–143
$\varepsilon_{t,in,n,rms}$ [π mm mrad]	0.20	0.20
$\varepsilon_{t,out,n,rms}$ [π mm mrad]	0.21	0.24
$\varepsilon_{l,out,n,rms}$ [π MeV deg]	0.10	0.11
L [m]	3.067	3.073
T [%]	99.1	99.1

IV. TOLERANCE FOR OFF-DESIGN INPUT BEAMS

In the real world, the manufacture and operation of accelerators cannot be ideal. Therefore, it is very important for a design approach to have sufficient tolerance for off-design situations.

The MEGLET RFQ has been tested for two cases with both different input beam intensities and different input emittances (see Table IV). The I_{in} and $\varepsilon_{t,in,n,rms}$ values for case 1 and case 2 are the same as those for the CERN Linac4 RFQ [22] and for the FAIR p-Linac RFQ [23], respectively. For a comparison, the nominal case (hereafter referred to as case 0) is also listed in the table. All three input beams have a waterbag-type distribution including 10^5 macroparticles. One difference is that the input beam

TABLE IV. Input beam intensities and emittances of the MEGLET RFQ for different cases.

Parameter	Case 0 (nominal case)	Case 1	Case 2
I_{in} [mA]	60	70	100
$\varepsilon_{\mathrm{t,in,n,rms}}$ [π mm mrad]	0.20	0.25	0.30

for case 1 has an input energy spread $\Delta W_{\mathrm{in}} = \pm 2\%$, because the simulation results for the Linac4 RFQ are based on this condition [28]. No matter for case 1 or case 2, the same MEGLET RFQ has been used, so all structure-related parameters, e.g., f, W_{in}, and U, have been kept fixed in the simulation.

Figure 10 compares the simulated transverse beam envelopes of the MEGLET RFQ for the three cases. From case 0 to case 2, I_{in} and $\varepsilon_{\mathrm{t,in,n,rms}}$ are increasing, and so does the beam size. The MEGLET RFQ has been designed for an input beam with $I_{\mathrm{in}} = 60$ mA and $\varepsilon_{\mathrm{t,in,n,rms}} = 0.2\ \pi$ mm mrad, so there are more beam losses in the two off-design cases. The simulated beam transmission efficiency for all transported particles is 97.6% and 89.4% for case 1 and case 2, respectively. For both cases, ~99% of the transported particles are well clustered around

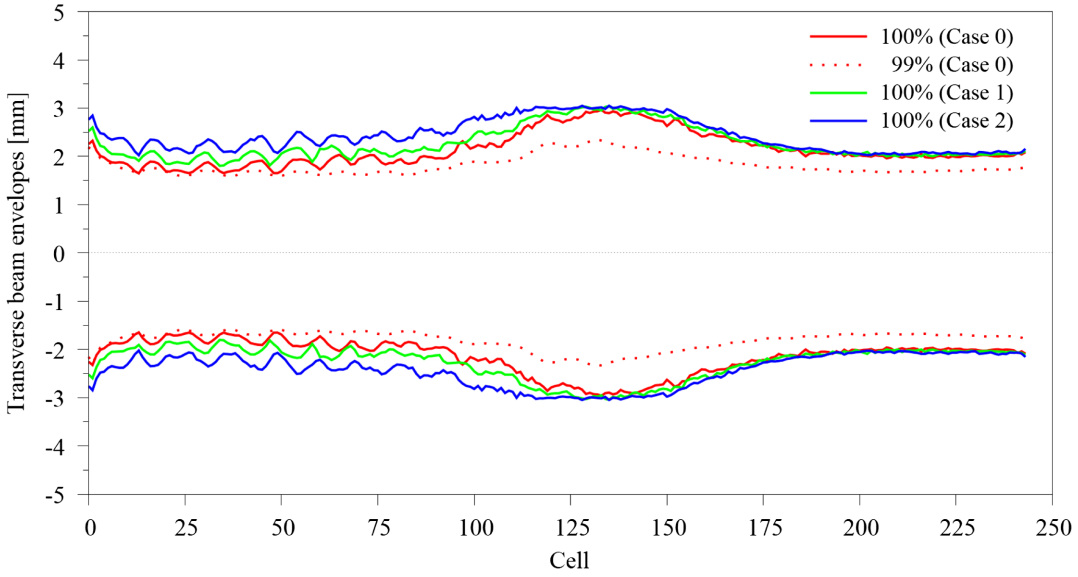

FIG. 10. Transverse beam envelopes of the MEGLET RFQ in different cases.

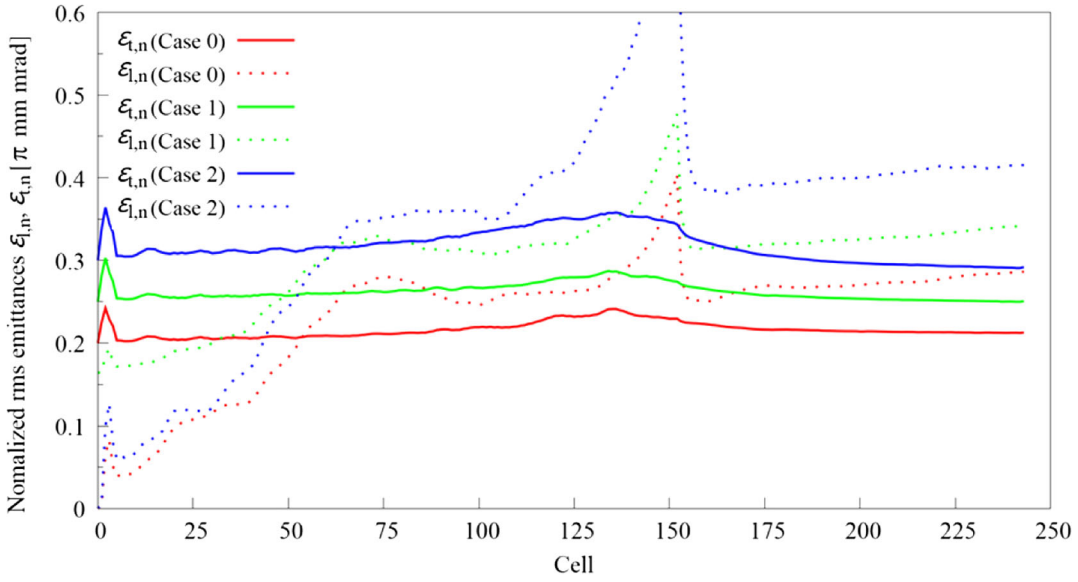

FIG. 11. Comparison of the longitudinal and transverse emittances (for 100% of particles) of the MEGLET RFQ in different cases.

TABLE V. Main simulation results of the MEGLET RFQ with off-design input beams.

Parameter	MEGLET case 1	CERN Linac4 [22,28]	MEGLET case 2	FAIR p-Linac [23]
Ion	H^+	H^-	H^+	H^+
f [MHz]	324	352.2	324	325.224
W_{in} [keV]	50 ($\pm$2%)	45 ($\pm$2%)	50	95
W_{out} [MeV]	3.0	3.0	3.0	3.0
U [kV]	75	78	75	88.43
I_{in} [mA]	70	70	100	100
$\varepsilon_{t,in,n,rms}$ [π mm mrad]	0.25	0.25	0.30	0.30
$\varepsilon_{t,out,n,rms}$ [π mm mrad]	0.25	0.25	0.29	0.33
$\varepsilon_{l,out,n,rms}$ [π MeV deg]	0.12	0.13	0.15	0.20
L [m]	3.067	3.06	3.067	3.3
T [%]	97.6	95.0	89.4	88.5

the synchronous particle with phase differences <30° and energy differences <30 keV.

The evolution of the longitudinal and transverse emittances for the three cases is shown in Fig. 11. As mentioned, the new approach uses two periods of emittance transfer after the initial bunching: (i) In the first transfer period, the transverse emittance increases and the longitudinal emittance decreases; (ii) In the second transfer period it is just the opposite. All transverse emittance curves show the two emittance-transfer periods clearly. For the longitudinal emittance, it can be seen that the green dashed curve (the $\varepsilon_{l,n}$ curve for case 1) does not start with 0 because of the $\pm$2% of input energy spread. In general, the three longitudinal emittance curves are still similar and from them the second emittance-transfer period can be distinctly seen. For case 1 and case 2, due to the larger input beam intensity and input emittance, the initial bunching cannot capture as many particles as in the nominal case. These small parts of particles outside of the separatrix make the first transfer period of the green and blue dashed curves less obvious.

The main simulation results for the two off-design cases as well as the corresponding values of the Linac4 RFQ and the p-Linac RFQ are listed in Table V. It can be seen that the MEGLET RFQ can still achieve comparable beam transmission efficiency as well as better output emittances by using lower intervane voltage, although the input beams are not optimum. It is worth mentioning that for the two off-design cases, the emittance ratio $\frac{\varepsilon_l}{\varepsilon_t}$ is still mainly inside the range from 0.9 to 1.4 along the MEGLET RFQ so that good performance in emittance growth has been kept.

V. CONCLUSION

To minimize the emittance growth caused by the longitudinal-transverse coupling, a new design approach so-called "MEGLET" is being proposed. On one hand, it follows a design guideline to hold the emittance ratio within the range of 0.9–1.4 for keeping the emittance transfer at low levels. On the other hand, it chooses a proper starting emittance ratio at the completion of the initial bunching and uses two emittance-transfer periods (in which the emittance transfer is in opposite directions) to bring the output emittance values back to the levels of the starting point.

The main differences between the EP method and the MEGLET approach can be summarized as follows: (i) The EP method emphasizes equal longitudinal and transverse oscillation energies, but for the MEGLET approach, close longitudinal and transverse emittance values are important. (ii) To minimize the emittance growth, the EP method tries to avoid the longitudinal-transverse coupling. On the contrary, the MEGLET approach allows and even takes advantage of low emittance transfer for achieving minimum emittance growth. (iii) For both methods, the tune trajectories will have oscillations when the tune trajectories are turning around in the tune space. An EP design usually has an intensive oscillation around the EP line, but in the MEGLET case, the oscillation will be much smaller and avoid the position where the main resonance peak can regrow. (iv) The MEGLET approach does not force the tune trajectories to stay on or closely around the EP line, so it allows changing the beam dynamics parameters more quickly with more freedom, which is helpful for leading to an efficient RFQ accelerator with good beam performance and lower rf power consumption. (v) Last but not least, the EP method usually requires a big variation in intervane voltage along the RFQ e.g., 61.3–143 kV for the J-PARC epRFQ, while the MEGLET approach adopts the typical way, i.e., to keep the intervane voltage constant throughout the RFQ, which is favorable for an easy rf tuning.

In addition, the new design approach can provide sufficient tolerance for off-design conditions. In the tests using two beams with both input beam intensity and input emittance much larger than the nominal values, the MEGLET RFQ still showed good beam performance especially from an emittance growth point of view.

ACKNOWLEDGMENTS

Sincere thanks go to Eugene Tanke for his friendly help in the development of useful data analysis tools.

[1] T. P. Wangler, *RF Linear Accelerators* (Wiley-VCH Verlag GmbH & Co. KG, Berlin, 2008).

[2] K. Schindl, Space charge, in *Proceedings of CAS–CERN Accelerator School: Intermediate Course on Accelerator Physics Zeuthen, Germany, 2003* (CERN, Geneva, 2006), p. 305.

[3] I. M. Kapchinskii and V. A. Teplyakov, Linear ion accelerator with spatially homogeneous strong focusing, Instrum. Exp. Tech. (USSR) **2**, 19 (1970).

[4] R. H. Stokes, K. R. Crandall, J. E. Stovall, and D. A. Swenson, RF quadrupole beam dynamics, in *Proceedings of PAC1979* (JACoW, San Francisco, 1979), p. 3469.

[5] P. M. Lapostolle, Effects of the space charge in a proton linear accelerator, CERN Report No. AR/Int. SG/65-15, 1965.

[6] F. J. Sacherer, RMS envelope equations with space charge, in *Proceedings of PAC1971* (JACoW, Chicago, 1971), p. 1105.

[7] P. M. Lapostolle and M. Weiss, Formulas and procedures useful for the design of linear accelerators, CERN Report No. CERN-PS-2000-001 (DR), 2000.

[8] R. Chasman, Numerical calculations of the effects of space charge on six dimensional beam dynamics in proton linear accelerators, in *Proceedings of LINAC1968* (JACoW, Long Island, 1968), p. 372.

[9] L. Smith, R. W. Chasman, K. R. Crandall, R. L. Gluckstern, T. Nishikawa, J. Haimson, and P. M. Lapostolle, Round table discussion of space charge and related effects, in *Proceedings of LINAC1968* (JACoW, New York, 1968), p. 433.

[10] R. A. Jameson, Equipartitioning in linear accelerators, in *Proceedings of LINAC1981* (JACoW, Santa Fe, New Mexico, 1981), p. 125.

[11] I. Hofmann, Emittance growth of beams close to the space charge limit, in *Proceedings of PAC1981* (JACoW, Washington, DC, 1981), p. 2399.

[12] I. Hofmann and I. Bozsik, Computer simulation of longitudinal transverse space charge effects in bunched beams, in *Proceedings of LINAC1981* (JACoW, Santa Fe, New Mexico, 1981), p. 116.

[13] I. Hofmann, Stability of anisotropic beams with space charge, Phys. Rev. E **57**, 4713 (1998).

[14] TraceWin code, http://irfu.cea.fr/dacm/logiciels/.

[15] C. Zhang and H. Podlech, Design approach for a 325 MHz, 3 MeV, 70–100 mA proton radio-frequency quadrupole accelerator with low emittance transfer, Nucl. Instrum. Methods Phys. Res., Sect. A **947**, 162756 (2019).

[16] C. Zhang and A. Schempp, Beam dynamics studies on a 200 mA proton radio frequency quadrupole accelerator, Nucl. Instrum. Methods Phys. Res., Sect. A **586**, 153 (2008).

[17] Y. Kondo, T. Morishita, and R. A. Jameson, Development of a radio frequency quadrupole linac implemented with the equipartitioning beam dynamics scheme, Phys. Rev. Accel. Beams **22**, 120101 (2019).

[18] Y. S. Cho, J. H. Jang, H. S. Kim, H. J. Kwon, and K. T. Seol, Design and fabrication of PEFP 350 MHz RFQ, in *Proceedings of the 2005 KNS Spring Meeting* (KNS, Jeju, Republic of Korea, 2005), p. 1056.

[19] H. F. Ouyang and S. Fu, Study of CSNS RFQ design, in *Proceedings of LINAC2006* (JACoW, Knoxville, 2006), p. 746.

[20] Y. Kondo, K. Hasegawa, T. Morishita, and R. A. Jameson, Beam dynamics design of a new radio frequency quadrupole for beam-current upgrade of the Japan Proton Accelerator Research Complex linac, Phys. Rev. ST Accel. Beams **15**, 080101 (2012).

[21] Q. Z. Xing, Y. J. Bai, J. Billen, J. C. Cai, C. Cheng, L. Du, Q. Du, T. B. Du, W. Q. Guan, X. L. Guan, Y. He, J. Li, J. Stovall, X. W. Wang, J. Wei, Z. F. Xiong, L. Young, H. Y. Zhang, and S. X. Zheng, A 3-MeV RFQ accelerator for the Compact Pulsed Hadron Source at Tsinghua University, Phys. Procedia **26**, 36 (2012).

[22] C. Rossi, P. Bourquin, J.-B. Lallement, A. M. Lombardi, S. Mathot, M. Timmins, G. Vandoni, M. Vretenar, S. Cazaux, O. Delferriere, M. Desmons, R. Duperrier, A. France, D. Leboeuf, and O. Piquet, The radiofrequency quadrupole accelerator for the Linac4, in *Proceedings of LINAC2008* (JACoW, Victoria, Canada, 2008), p. 157.

[23] M. Syha, H. Hähnel, U. Ratzinger, and M. Schuett, New beam dynamics simulations for the FAIR p-linac RFQ, in *Proceedings of IPAC2019* (JACOW, Melbourne, Australia, 2019), p. 921.

[24] Manual of the LANL RFQ design codes, LANL Report No. LA-UR-96-1836, revised 2005.

[25] I. Hofmann and O. Boine-Frankenheim, Parametric instabilities in 3D periodically focused beams with space charge, Phys. Rev. Accel. Beams **20**, 014202 (2017).

[26] T. Morishita and Y. Kondo, Electromagnetic design and tuning of the four-vane radio frequency quadrupole with nonuniform intervane voltage profile, Phys. Rev. Accel. Beams **23**, 111003 (2020).

[27] T. Morishita, Y. Kondo, T. Hori, S. Yamazaki, K. Hasegawa, K. Hirano, H. Oguri, A. Takagi, T. Sugimura, and F. Naito, High-power test results of the RFQ III in J-PARC linac, in *Proceedings of LINAC2014* (JACoW, Geneva, Switzerland, 2014), p. 649.

[28] C. Rossi (private communication).